Chapter 8
Protein Dynamics

High-resolution NMR spectroscopy has become a unique and powerful approach with atomic resolution not only for determining structures of biological macromolecules but also for characterizing the overall and internal rotational motions in proteins. The dynamic behavior of proteins at different timescales can be monitored experimentally by different methods because it is difficult, if not impossible, to completely characterize all motional processes by a single approach. Nuclear spin relaxation measurement provides information on fast motions on the timescales of picosecond to nanosecond (laboratory frame nuclear spin relaxation experiments), and slow motions on the timescales of microsecond to millisecond (rotating frame nuclear spin relaxation measurements), whereas magnetization exchange spectroscopy deals with motions on the timescales of millisecond to second. This chapter focuses on the experiments and data analysis for heteronuclear spin relaxation approaches used to characterize the dynamic processes of proteins in solution.

Key questions to be addressed include the following:

1. What is spectral density?
2. What is correlation time?
3. How can they be interpreted to describe protein dynamics?
4. What types of nuclear interactions can be used for dynamics study?
5. How can these interactions be used to obtained spectral density and correlation time?
6. How are T_1, T_2, and NOE measured?
7. How are the relaxation parameters derived from the experimental data?
8. What timescales of protein internal motions can NMR be used to study?
9. How are the results of relaxation parameters presented to illustrate the protein motions?
10. How are the experiments for protein dynamics measurements set up?

Q. Teng, *Structural Biology: Practical NMR Applications*,
DOI 10.1007/978-1-4614-3964-6_8,

8.1 Theory of Spin Relaxation in Proteins

The relaxation rates of proteins are affected primarily by dipolar interactions and chemical shift anisotropy (CSA). For ^{2}H labeled proteins, the ^{2}H quadrupolar interaction also contributes to the relaxation rates. The overall relaxation rates are the linear combination of all rates of the interactions. The relaxation rates can be expressed in terms of the combination of spectral density functions (Abragam 1961; Kay et al. 1989). For an isolated XH spin system, the relaxation rate constants of the X spin (^{15}N or ^{13}C) caused by the dipolar interaction of the X spin with the ^{1}H spin and by the magnetic shielding arising from the CSA interaction of the X spin are given by:

$$\begin{aligned} R_1 &= R_1^{\mathrm{D}} + R_1^{\mathrm{CSA}} \\ &= \frac{d^2}{4}\left[6J(\omega_{\mathrm{H}}+\omega_{\mathrm{X}}) + J(\omega_{\mathrm{H}}-\omega_{\mathrm{X}}) + 3J(\omega_{\mathrm{X}})\right] + c^2 J(\omega_{\mathrm{X}}) \end{aligned} \tag{8.1}$$

$$\begin{aligned} R_2 &= R_2^{\mathrm{D}} + R_2^{\mathrm{CSA}} \\ &= \frac{d^2}{8}\left[6J(\omega_{\mathrm{H}}+\omega_{\mathrm{X}}) + 6J(\omega_{\mathrm{H}}) + J(\omega_{\mathrm{H}}-\omega_{\mathrm{X}}) + 3J(\omega_{\mathrm{X}}) + 4J(0)\right] \\ &\quad + \frac{c^2}{6}\left[3J(\omega_{\mathrm{X}}) + 4J(0)\right] \end{aligned} \tag{8.2}$$

$$\sigma_{\mathrm{XH}} = \frac{d^2}{4}\left[6J(\omega_{\mathrm{H}}+\omega_{\mathrm{X}}) - J(\omega_{\mathrm{H}}-\omega_{\mathrm{X}})\right] \tag{8.3}$$

in which R_1, R_2, and σ_{XH} are the rate constants of spin–lattice relaxation, spin–spin relaxation, and cross-relaxation, respectively, which are dependent on the spectral density functions evaluated at five frequencies ($\omega_{\mathrm{H}} = \omega_{\mathrm{X}}$, ω_{H}, $\omega_{\mathrm{H}} - \omega_{\mathrm{X}}$, ω_{X}, and 0); $d = \mu_0 \hbar \gamma_{\mathrm{X}} \gamma_{\mathrm{H}} \langle r_{\mathrm{XH}}^{-3} \rangle / 8\pi$; μ_0 is the permeability of vacuum ($4\pi \times 10^{-7}$ T mA); $\hbar$ is reduced Plank's constant; r_{XH} is the XH bond length; γ_{X} and γ_{H} are the gyromagnetic ratios; $c = \Delta\sigma\omega_{\mathrm{X}}/\sqrt{3}$; $\Delta\sigma$ is the CSA of the X spin with the assumption that the chemical shift tensor is axially symmetrical, which has been demonstrated to be valid for peptide bond ^{15}N with $\Delta\sigma = -160$ to -170 ppm (Hiyama et al. 1988), $\Delta\sigma = 25 - 35$ ppm for peptide carbonyl ^{13}C and $\Delta\sigma =$ 30 ppm for $^{13}C^{\alpha}$ (Ye et al. 1993). The R_1 and R_2 rate constants can be directly determined experimentally ($R_1 = 1/T_1$ and $R_2 = 1/T_2$), whereas σ_{XH} is determined from stead-state {^{1}H}-X NOE via the relationship (Kay et al. 1989; Yamazaki et al. 1994):

$$\sigma_{\mathrm{XH}} = \frac{d^2}{4}\left[6J(\omega_{\mathrm{H}}+\omega_{\mathrm{X}}) - J(\omega_{\mathrm{H}}-\omega_{\mathrm{X}})\right] = \frac{\gamma_{\mathrm{X}}}{\gamma_{\mathrm{H}}} R_1(\mathrm{NOE}-1) \tag{8.4}$$

which can be recast to:

$$\mathrm{NOE} = 1 + \frac{\sigma_{\mathrm{XH}}}{R_1}\frac{\gamma_{\mathrm{X}}}{\gamma_{\mathrm{H}}} = 1 + \frac{d^2}{4R_1}\frac{\gamma_{\mathrm{X}}}{\gamma_{\mathrm{H}}}\left[6J(\omega_{\mathrm{H}}+\omega_{\mathrm{X}}) - J(\omega_{\mathrm{H}}-\omega_{\mathrm{X}})\right] \tag{8.5}$$

Without any assumptions, the spectral density functions at the five frequencies cannot be determined from the three experimentally determined relaxation rate constants by measuring T_1, T_2, and NOE. Assumptions must be made so that only three unknowns need to be determined from the three known values.

There are various mathematical models for mapping the spectral density functions (Wittebort et al. 1978; London 1980), of which the model-free analysis is widely used to obtain information about site-specific internal motions of proteins (Lipari and Szabo 1982a, b; Clore et al. 1990a, b; Dayie et al. 1996; Palmer 2001). Rather than fitting the experimental data to any specific physical models, the method depends on the mathematical analysis of spectral density functions by assuming two types of motions contributing to the dynamic process for isotropically tumbling proteins: overall tumbling of the protein as a whole and internal dynamics for the heteronuclear bonds. Therefore, the analysis characterizes the amplitude and rate of internal dynamics for individual chemical bond vectors (e.g., peptide NH bond) via model-free order parameters S (or the generalized order parameter), the overall rotational correlation time τ_m (or global correlation time) and effective correlation time τ_e according to the relationship:

$$J(\omega) = \frac{2}{5}\left[\frac{S^2\tau_m}{1+(\omega\tau_m)^2} + \frac{(1-S^2)\tau}{1+(\omega\tau)^2}\right] \tag{8.6}$$

in which τ is given by

$$\tau = \left(\frac{1}{\tau_m} + \frac{1}{\tau_e}\right)^{-1} \tag{8.7}$$

The effective correlation time τ_e is the internal correlation time for motions of a bond vector in a molecular frame. The squared generalized order parameter S^2 measures the degree of spatial restriction of the bond vector in a molecular frame, which provides information about the angular amplitude of the internal motions of bond vectors. If the bond vector diffuses in a cone with an angle θ defined by the diffusion tensor and the equilibrium orientation of the bond vector, S^2 is highly sensitive to the cone angle in the range from 0° to 75°, and decreases dramatically as the cone angle increases (Ishima and Torchia 2000; Fig. 8.1). The value of θ may vary from 1 when the bond is rigid to 0 when the internal motion is completely isotropic. The overall rotational correlation time τ_m characterizes the molecular tumbling whereas internal correlation time τ_e describes the internal dynamics.

The model-free formalism has been extended to include internal motions both on a fast timescale and slow timescale (Clore et al. 1990a, b; Farrow et al. 1994). The spectral density function described by the extended model-free formalism is given by:

$$J(\omega) = \frac{2}{5}\left[\frac{S^2\tau_m}{1+(\omega\tau_m)^2} + \frac{(S_f^2-S^2)\tau}{1+(\omega\tau)^2}\right] \tag{8.8}$$

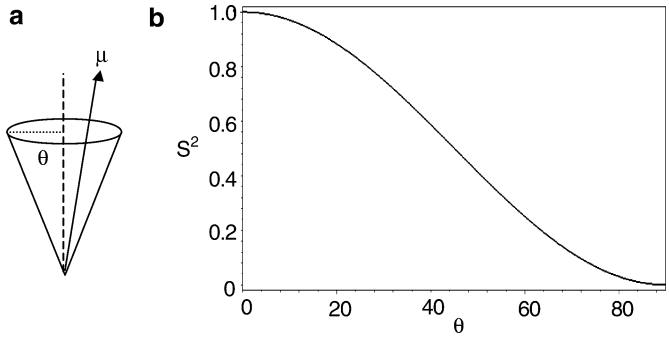

Fig. 8.1 Model-free parameters for characterizing dynamics of proteins. (**a**) Relationship of bond vector μ and the angular amplitude of the internal motion of the bond with respect to its equilibrium position, defined by θ. (**b**) The value of the squared generalized order parameter S^2 changes as a function of θ described by (8.26) for diffusion in a cone as shown in (**a**) (reproduced with permission from Ishima and Torchia (2000), Copyright © 2000 Nature Publishing Group)

in which

$$\tau = \left(\frac{1}{\tau_m} + \frac{1}{\tau_s}\right)^{-1} \tag{8.9}$$

and τ_s is the internal correlation time for slow motion, S^2, the squared generalized order parameter $= S_f^2 S_s^2$, and S_f^2 and S_s^2 are the squared generalized order parameters characterizing the fast and slow internal motions, respectively.

The squared generalized order parameter S^2 and correlation times τ_m, τ_e, τ_f, and τ_s can be determined by two different types of approaches. The first type of approach relies on valid assumptions to simply the equations for spectral density functions, including the R_2/R_1 ratio method and the constant high-frequency spectral density method. The second type is based on the optimization of fitting the data to obtain the dynamic parameters, which tends to generate quantitative analysis. From the expressions for R_2 and R_1, the ratio R_2/R_1 is given by (Kay et al. 1989; Mayo et al. 2000):

$$\frac{R_2}{R_1} = \frac{d^2[6J(\omega_H + \omega_X) + 6J(\omega_H) + J(\omega_H - \omega_X)] + (d^2 + (4c^2/3))[3J(\omega_X) + 4J(0)]}{2d^2[6J(\omega_H + \omega_X) + J(\omega_H - \omega_X) + 3J(\omega_X)] + c^2 J(\omega_X)} \tag{8.10}$$

R_1 and R_2 are the relaxation rates for each backbone ^{15}N spin. The R_2/R_1 ratio method assumes that internal motions of bond vectors are sufficiently faster than overall tumbling ($\tau_e \leq 200$ ps) and have low amplitude ($S^2 \geq 0.5$) so that the ratio of ^{15}N R_2 and R_1 relaxation rate constants is essentially independent of the internal correlation time τ_e. Since τ_e is relatively small based on the assumption, the spectral

density function $J(\omega)$ primarily relies only on single correlation time—overall correlation time τ_m, which simplifies the expression to the form of:

$$J(\omega) = \frac{2}{5} \frac{S^2 \tau_m}{1 + (\omega \tau_m)^2} \tag{8.11}$$

By replacing $J(\omega)$ in (8.10) with (8.11), the R_2/R_1 ratio is independent of S^2 and the overall correlation time τ_m can be determined via computer minimization of the deviation of the following equation using all observed values of the R_2/R_1 ratio at different static magnetic field strengths for each backbone ^{15}N site:

$$\tau_m = \frac{1}{\omega_N} \sqrt{\frac{6R_2}{R_1} - 17} \tag{8.12}$$

The R_2 and R_1 constants are sensitive to motions on different timescales. R_1 is sensitive to the dynamics on the timescale of picosecond to microsecond, whereas R_2 is sensitive to the motions on both the picosecond to microsecond and microsecond to millisecond timescales. For the ^{15}N spins that have a R_2/R_1 ratio below the average value by a difference larger than the standard deviation, local conformational averaging at a rate comparable to the chemical shift difference between the conformational forms is assumed to be responsible for the shortening of the T_2 relaxation. For the ^{15}N sites at which the R_2/R_1 ratio is above the average value by a difference larger than the standard deviation, the prolongation of T_1 is caused by a motion on a timescale comparable to τ_m. The squared generalized order parameter S^2 for an individual site can in turn be obtained using the expression either for R_1 or R_2 ((8.1) or (8.2)) with the average value of τ_m. In practice, S^2 is obtained using R_1 and NOE (8.1) without T_2 relaxation data because the measured T_2 may contain contributions from other mechanisms, such as slow motions, scalar relaxation, chemical exchange, antiphase magnetization, pulse imperfection, off-resonance effect of the CPMG pulse train, cross-correlation of dipolar/CSA interactions, etc.

Another simplification method is to approximate the spectral density functions in (8.1)–(8.3) to the first order as a single term $\alpha J(\beta\omega)$, in which α and β are constants (Farrow et al. 1995; Ishima and Nagayama 1995a, b), by assuming that it can be described by a linear combination of the contributions from overall rotation and internal motions. The spectral density function is given by:

$$J(\omega) = \frac{\lambda_1}{\omega^2} + \lambda_2 \tag{8.13}$$

in which the first term and second term are the contributions from overall rotation and internal motions, respectively. The rate constants consisting of the linear combination of the five spectral densities may then be simplified as:

$$R_1 = \frac{d^2}{4} [7J(\beta_1 \omega_H) + 3J(\omega_X)] + c^2 J(\omega_X) \tag{8.14}$$

$$R_2 = \frac{d^2}{8}[13J(\beta_2\omega_H) + 3J(\omega_X) + 4J(0)] + \frac{c^2}{6}[3J(\omega_X) + 4J(0)] \tag{8.15}$$

$$\text{NOE} = 1 + \frac{5d^2}{4R_1}\frac{\gamma_X}{\gamma_H}J(\beta_3\omega_H) \tag{8.16}$$

in which β_1, β_2, and β_3 can be obtained using the relationships (Farrow et al. 1995):

$$\frac{6}{(\omega_H + \omega_X)^2} + \frac{1}{(\omega_H - \omega_X)^2} = \frac{7}{(\beta_1\omega_X)^2} \tag{8.17}$$

$$\frac{6}{(\omega_H + \omega_X)^2} + \frac{6}{\omega_H^2} + \frac{1}{(\omega_H - \omega_X)^2} = \frac{13}{(\beta_2\omega_X)^2} \tag{8.18}$$

$$\frac{6}{(\omega_H + \omega_X)^2} - \frac{1}{(\omega_H - \omega_X)^2} = \frac{5}{(\beta_3\omega_H)^2} \tag{8.19}$$

The equations yield $\beta_1 = 0.921$, $\beta_2 = 0.955$, and $\beta_3 = 0.87$ for ^{15}N spin relaxation, and $\beta_1 = 1.12$, $\beta_2 = 1.06$, and $\beta_3 = 1.56$ for ^{13}C spin relaxation. The method does not assume that the molecular tumbling is isotropic. The spectral density functions are first obtained from experimental data of T_1, T_2, and NOE, and then used to determine the squared generalized order parameter and correlation times. For backbone ^{15}N spins, the value of $J(0.78\omega_H)$ is calculated directly from the observed values of T_1 and NOE using the equation:

$$J(0.87\omega_H) = \frac{4\sigma_{NH}}{5d^2} \tag{8.20}$$

in which d is defined as in (8.1) and σ_{NH} is given in (8.4).

The spectral density functions for the other four frequencies are extracted either by assuming $J(\omega) \propto 1/\omega^2$ in the range of $\omega_H \pm \omega_N$, or from the values of $J(0.78\omega)$ obtained at different field strengths. When $J(\omega_H) \propto 1/\omega_H^2$, $J(\beta_i\omega_H)$ can be estimated according to (Farrow et al. 1995)

$$J(\beta_i\omega_H) \approx \left(\frac{0.87}{\beta_i}\right)^2 J(0.87\omega_H) \tag{8.21}$$

in which $i = 1$, 2 or 3. Therefore, $J(\omega)$ at 0 and ω_N are given by:

$$J(0) = \frac{6R_2 - 3R_1 - 2.72\sigma_{NH}}{3d^2 + 4c^2} \tag{8.22}$$

$$J(\omega_N) = \frac{4R_1 - 5\sigma_{NH}}{3d^2 + 4c^2} \tag{8.23}$$

If values of $J(0.78\omega_H)$ obtained at different field strengths are employed, $J(\beta_i\omega_H)$ can be estimated from:

$$J(\beta_i\omega_H) \approx J(0.87\omega_H) - (\beta_i - 0.87)\omega_H \frac{J(0.87\omega_H) - J(0.87\omega'_H)}{0.87(\omega_H - \omega'_H)} \tag{8.24}$$

in which ω'_H is the proton Larmor frequency at which $J(0.78\omega'_H)$ is obtained and ω'_H is different than ω_H.

The second type of method utilizes extensive optimization of data fitting globally or locally for all peptide residues by minimizing an error function to obtain the overall correlation time τ_m (Dellwo and Wand 1989; Palmer et al. 1991; Mandel et al. 1995). For global fitting, the global error function may have a form of:

$$\chi^2 = \sum_{j=1}^{M} \left[\left(\frac{R_{1j}^{obs} - R_{1j}^{cal}}{\lambda_{R_{1j}}} \right)^2 + \left(\frac{R_{2j}^{obs} - R_{2j}^{cal}}{\lambda_{R_{2j}}} \right)^2 + \left(\frac{NOE_j^{obs} - NOE_j^{cal}}{\lambda_{NOE_j}} \right)^2 \right] \tag{8.25}$$

in which M is the number of residues for which the relaxation parameters have been measured; λ is the standard deviation in R_1, R_2 or NOE for residue j; the superscripts obs and cal denote the observed and calculated relaxation parameters, respectively. The minimization can also be done for a local error function with $M = 1$ for an individual residue. In either case, an array of presumed values of correlation time is selected for fitting the parameters (S^2 and τ_e) for internal motion. The correlation time τ_m is identified when the sum of the deviations between the observed and calculated relaxation parameters has reached a minimum. Using the data observed at different field strengths reduces the fitting error and improves the quality of the extracted dynamic parameters.

The squared generalized order parameter, S^2, is the measure of the orientational distribution of internal motions by the bond vector in the molecular frame. For the model describing the internal motion of bond vector as a restricted diffusion in a cone, the quantity S^2 is given by (Lipari and Szabo 1982a, b):

$$S^2 = \left[\frac{\cos\theta(1 + \cos\theta)}{2} \right]^2 \tag{8.26}$$

in which θ is the angle between the bond vector and the diffusion cone as defined in Fig. 8.1a, which characterizes the angular amplitude of the internal motion. When θ is equal to zero, the motion of the vector is restricted to the fixed orientations and S^2 is unity, the maximum value. As θ increases, S^2 decreases rapidly and the motion of the bond vector becomes less restricted. The motion becomes completely isotropic when θ is 75°, leading to an S^2 of almost zero.

In addition to S^2, the internal correlation time τ_e also is an important quantity for characterizing the internal motions. Although quantitative interpretation of τ_e relies on how realistic the model is to describe the motion, the determined value provides a

qualitative insight about the rate of internal motion. However, as (8.11) ($J(\omega) \propto S^2$, τ_m, τ_e) indicates, τ_e can precisely be characterized only over a very narrow frequency range. In general, the accurate determination of τ_e based on the equation is limited in the range of >30 ps (slower than 30 ps) and $\ll\tau_m$ (much faster than τ_m; Palmer 2001). The accuracy of τ_e determination can be significantly increased by applying the relaxation data obtained for additional nuclei besides ^{15}N, such as ^{13}C and/or ^{2}H.

For quadrupolar interaction of spin-1 nuclei such as ^{2}H bound to ^{13}C, the quadrupolar relaxation is much more efficient than the dipolar interaction and hence the relaxation rate constants contain only quadrupolar relaxation and are expressed by (Wittebort and Szabo 1978):

$$R_1 = \frac{3C_Q^2}{16}[2J(2\omega_D) + J(\omega_D)] \tag{8.27}$$

$$R_2 = \frac{3}{32}C_Q^2[2J(2\omega_D) + 5J(\omega_D) + 3J(0)] \tag{8.28}$$

in which $C_Q = e^2qQ/\hbar$ is the quadrupolar coupling constant, e is the charge of an electron, q is the principal value of the electric field gradient tensor, Q is the nuclear quadrupolar moment, ω_D is the ^{2}H frequency, and $J(0)$, $J(\omega_D)$ and $J(2\omega_D)$ correspond to the spectral density function at the zero-, single- and double-quantum ^{2}H frequencies. Generally, the assumption that the principal axis of the electric field gradient tensor is collinear with the C–^{2}H bond vector is valid except for methyl groups.

Cross-correlation between different nuclear interactions may potentially complicate the determination of molecular dynamics based on spin relaxation measurement. For an isolated HX spin system, the relaxation rates including cross-correlation (or cross correlated relaxation) of dipolar and CSA interactions are different for the downfield and upfield lines of an ^{15}N or ^{13}C doublet (Goldman 1984; Bull 1992):

$$R^+ = R + R^c \quad \text{and} \quad R^- = R - R^c \tag{8.29}$$

in which $R^{\pm}$ are the rate constants for the upfield (right) and downfield (left) line, respectively, R is defined as in (8.1) and (8.2), and R^c is the rate from the cross-correlation between the two interactions. The influence of the cross-correlation on the spin relaxation is usually removed during spin relaxation rate measurements by applying a continuous inversion of the proton resonance during the relaxation periods. However, this interaction provides useful information in such cases as when the relative orientation of the CSA tensor with respect to the dipolar interaction or bond vector is known. For an axially symmetric CSA tensor, the rate constants from cross-correlation with the dipolar interaction can be described in terms of:

$$R_1^C = -\sqrt{3}dcP_2(\cos\theta)J(\omega_X) \tag{8.30}$$

$$R_2^{\mathrm{C}} = -\frac{\sqrt{3}}{6} dc P_2(\cos\theta)[3J(\omega_{\mathrm{X}}) + 4J(0)] \tag{8.31}$$

in which R_1^{C} and R_2^{C} are the longitudinal and transverse relaxation rates of the cross-correlation, respectively, c and d are the constants defined in (8.1), $P_2(x) = (3x^2 - 1)/2$ is the second Legendre polynomial, and θ is the angle between the HX bond vector and the symmetric axis of the CSA tensor. By measuring R_1 and R_2 in the absence and presence of ^{1}H decoupling during the relaxation period T, the contribution from the cross-correlation of the heteronuclear dipole and CSA interactions can be obtained according to the expression for R^+ or R^-.

The spin–spin relaxation can also be affected by additional internal motions induced by chemical exchange processes such as those arising from microsecond to millisecond exchange of spins between magnetic environments during the δ delays of a CPMG sequence. Consequently, the $J(0)$ determined according to (8.30) and (8.31) or (8.22) may not be accurate. The exchange rate constant R_{ex} was proposed to add to the expression of transverse relaxation rate R_2:

$$R_2 = R_2^{\mathrm{D}} + R_2^{\mathrm{CSA}} + R_{\mathrm{ex}} \tag{8.32}$$

The exchange rate can be determined by its magnetic field dependence with the assumption $R_{\mathrm{ex}} = \lambda_{\mathrm{ex}} B_0^2$, in which λ_{ex} is a constant (Peng and Wagner 1995; Phan et al. 1996; Kroenke et al. 1999):

$$R_2 - \frac{1}{2}R_1 = \frac{d^2}{4}[3J(\omega_{\mathrm{H}}) + 2J(0)] + \left[\frac{2}{9}\gamma_{\mathrm{X}}^2 \Delta\sigma^2 J(0) + \lambda_{\mathrm{ex}}\right] B_0^2 \tag{8.33}$$

By fitting the relaxation data obtained at different field strengths vs. the squared static field strength B_0^2, R_{ex} as well as $J(0)$ can be calculated from the intercept since $J(\omega_{\mathrm{H}})$ is determined from τ_{m} and τ_{e} by the methods described previously. Alternatively, the transverse rates of the dipole/CSA cross-correlation, which are not affected by chemical exchange processes, can be used to directly identify the contribution to R_2 arising from chemical exchange effects. The spectral density function $J(0)$ can be represented in terms of R_1^{C} and R_2^{C}:

$$J(0) = -\frac{2\sqrt{3}}{dcP_2(\cos\theta)}\left(R_2^{\mathrm{C}} - \frac{1}{2}R_1^{\mathrm{C}}\right) \tag{8.34}$$

Once $J(0)$ is obtained, R_{ex} can be determined from the slope of fitting $(R_2 - \frac{1}{2}R_1)$ vs. B_0^2 in (8.33).

For anisotropically tumbling proteins with axially symmetric rotational diffusion tensors, the model-free spectral density functions are given by (Brüschweiler et al. 1995):

$$J(\omega) = \frac{2}{5}\sum_{j=0}^{2} A_j \left[\frac{S^2\tau_j}{1 + (\omega\tau_j)^2} + \frac{(1 - S^2)\tau'_j}{1 + (\omega\tau'_j)^2}\right] \tag{8.35}$$

in which $1/\tau'_j = (1/\tau_j) + (1/\tau_e)$; $1/\tau_j = 6D_\perp - j^2(D_\perp - D_\parallel)$; $D_\perp$ and $D_\parallel$ are the perpendicular and parallel components of the axially symmetric diffusion tensor; $A_0 = P_2(\cos\theta)/2$; $A_1 = 3\cos^2\theta\sin^2\theta$; $A_2 = (3\sin^4\theta)/4$; and θ is the angle between the average orientation of the bond vector and the parallel component of the axially symmetric diffusion tensor (Fig. 8.1a), which is obtained from the known structure of the protein. For isotropic rotational motions, $D_\perp = D_\parallel$. Then, $\tau_j = \tau_m$ and $\tau'_j = \tau$, and $\sum A_j = 1$. Equation (8.35) reduces to the model-free expression for isotropically tumbling proteins.

8.2 Experiments for Measurement of Relaxation Parameters

The measurement of spin relaxation rates is achieved by carrying out a series of 2D heteronuclear HSQC- or HMQC-type experiments. The pulse sequences for T_1 and T_2 relaxation measurement include a relaxation period inserted either before or after the t_1 evolution period, whereas for heteronuclear NOE measurement, the cross-relaxation period (saturation period) is incorporated into the preparation period in the 2D steady-state NOE sequence.

8.2.1 T_1 Measurement

8.2.1.1 Water Flip-Back Sensitivity-Enhanced T_1 HSQC

The inversion technique described in Chap. 1 is widely used to measure the longitudinal relaxation time T_1. The scheme (Fig. 8.2a, Farrow et al. 1994; Kay et al. 1992) consists of a 180° inversion pulse that inverts the heteronuclear magnetization S_z to $-S_z$, a relaxation period T during which the magnetization relaxes along the z axis, and a 90° pulse to create observable transverse magnetization for detection. For T_1 measurement, this relaxation block is inserted to the seHSQC sequence before the t_1 evolution time. The HSQC is slightly different than the ^{15}N seHSQC, in which double refocused INEPT-type sequences are utilized to transfer the magnetization from the directly bound proton to the heteronucleus and back to the proton for observation via the reversed refocused-INEPT pathway. In-phase magnetization is generated before the relaxation period rather than the antiphase coherence created in the conventional seHSQC sequence. The selective water flip-back pulse is used to ensure that the water magnetization remains along the z axis during the experiment so that saturation transfer is minimized. ^{1}H decoupling consisting of 180° pulses is used during the relaxation period T to eliminate effects of the cross-correlation between dipolar and CSA interactions. The decoupling pulse train should not perturb the longitudinal water magnetization, and consists of shaped selective 180° pulses such as cosine-modulated 180° pulses.

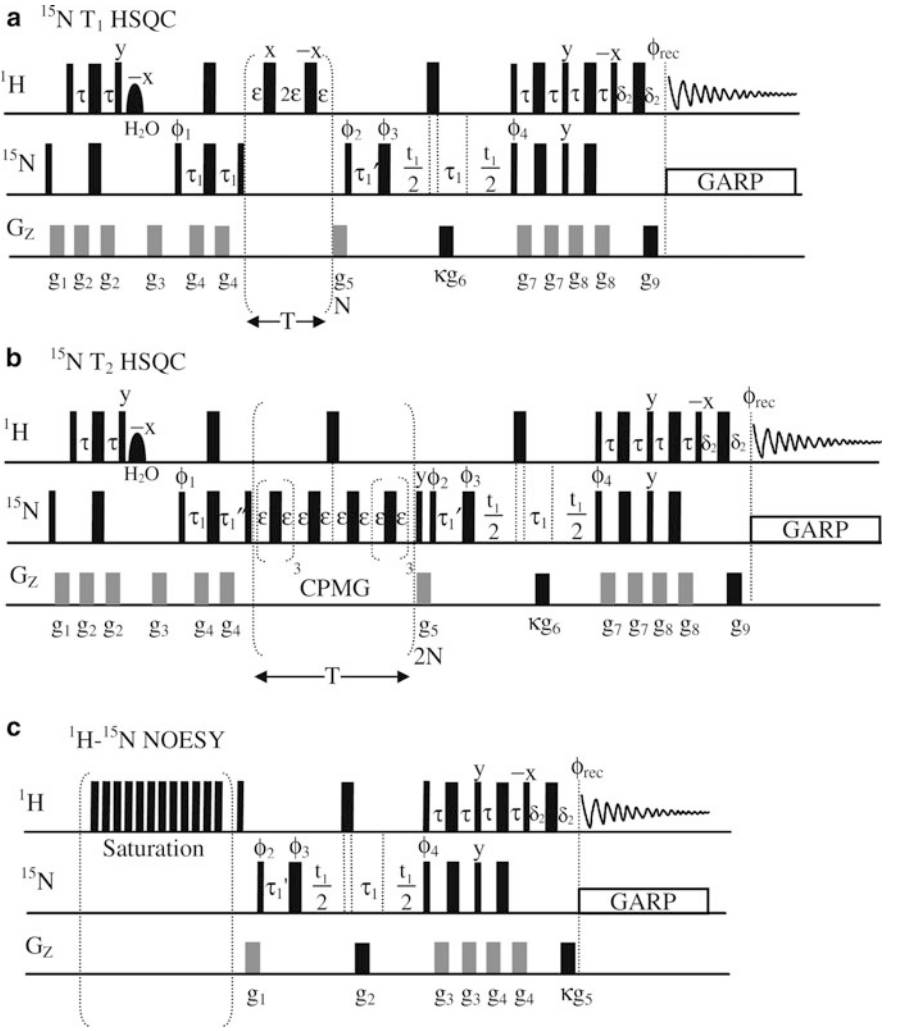

Fig. 8.2 Pulse sequences for spin relaxation measurements of ^{15}N (**a**) T_1, (**b**) T_2 relaxation times and (**c**) NOE value with sensitivity enhancement and gradient coherence selection. $R_1 = 1/T_1$ and $R_2 = 1/T_2$. In all experiments, narrow and *wide bars* represent 90° and 180° pulses, respectively; water flip-back selective pulses are shown in *rounded small bars* which are 1.8-ms *rectangular pulses*. Unless otherwise specified, all pulses have x phase. The coherence selection is achieved by the black gradients and $\kappa = \pm 1$ and stored in different memory locations. For PEP sensitivity enhancement two FIDs are recorded by inverting the phase ϕ_4 and the sign of κ in second experiment for every t_1. The T_1 and T_2 relaxation data are recorded by a series of experiments with different relaxation periods T. In all experiments, the delay τ is set to 2.25 ms, τ_1 to 2.75 ms, $\tau'_1 = \tau_1 + 2\text{pw}$ in which pw is ^{1}H 90° pulse length, $\tau''_1 = \tau_1 + (2/\pi)\text{pw}_\text{N}$ in which pw_N is ^{15}N 90° pulse length, and δ_2 to 0.5 ms. Recycle delays are 1.5 s for T_1 and T_2 experiments and 5 s for NOE and NONOE experiments. For the T_1 experiment (**a**) the gradient pulses are applied as $g_1 = 1$ ms, 5 G cm^{-1}, $g_2 = 0.5$ ms, 4 G cm^{-1}, $g_3 = 2$ ms, 10 G cm^{-1}, $g_4 = 0.5$ ms, 8 G cm^{-1}, $g_5 = 1$ ms, 10 G cm^{-1}, $g_6 = 1.25$ ms, 30 G cm^{-1}, $g_7 = g_8 = 0.5$ ms, 4 G cm^{-1}, $g_9 = 0.125$, 27.8 G cm^{-1}. The phase cycle is $\phi_1 = x, -x$, $\phi_2 = y$, +States–TPPI, $\phi_3 = 2(x), 2(y), 2(-x), 2(-y)$, $\phi_4 = x$, and

The relaxation-encoded ^{15}N magnetization consequently evolves with the scalar coupling being refocused during the t_1 evolution period. During the "back" transfer pathway, the relaxation-encoded frequency-labeled ^{15}N magnetization is transferred back to the directly bound proton and a PEP sequence is used to increase the sensitivity by as much as a factor of $\sqrt{2}$ compared to the unenhanced spectrum. Quadrature detection in the F_1 dimension is obtained by shifting the phases of ϕ_2 and the receiver for each FID using the States–TPPI method (see Sect. 4.10.2). The ^{15}N 90° pulse combined with the gradient at the beginning of the pulse sequence is used to ensure that the initial magnetization originates only from amide proton spins. The magnetization transfer during the experiment can be described in terms of product operators:

$$\mathrm{H}_z \xrightarrow{\left(\frac{\pi}{2}\right)\mathrm{H}_x} -\mathrm{H}_y \xrightarrow{\tau \to \pi(\mathrm{H}_x+\mathrm{N}_x) \to \tau \to \left(\frac{\pi}{2}\right)(\mathrm{H}_y+\mathrm{N}_x)} -2\mathrm{H}_z\mathrm{N}_y \tag{8.36}$$

$$\xrightarrow{\tau_1 \to \pi(\mathrm{H}_x+\mathrm{N}_x) \to \tau_1} \mathrm{N}_x \xrightarrow{\left(\frac{\pi}{2}\right)\mathrm{N}_y} -\mathrm{N}_z \xrightarrow{T} -\xi\mathrm{N}_z \tag{8.37}$$

The factor ξ is the T dependence of the magnetization (signal amplitude), which is given by:

$$\xi = 1 - 2\mathrm{e}^{-T/T_1} = 1 - 2\mathrm{e}^{-TR_1} \tag{8.38}$$

The ^{1}H–^{15}N scalar coupling is decoupled during the relaxation period T. After being brought to the transverse plane by the following 90° ^{15}N pulse, the ^{15}N magnetization evolves while the heteronuclear scalar coupling is decoupled during the t_1 period. The ^{15}N magnetization is transferred back to proton during the evolution of $2\tau_1$ period.

$$\begin{aligned} &-\xi\mathrm{N}_z \xrightarrow{\left(\frac{\pi}{2}\right)\mathrm{N}_x} \xi\mathrm{N}_y \\ &\xrightarrow{t_1} \xi\mathrm{N}_y \cos\left(\Omega_\mathrm{N} t_1\right) - \xi\mathrm{N}_x \sin\left(\Omega_\mathrm{N} t_1\right) \end{aligned} \tag{8.39}$$

Fig. 8.2 (continued) receiver phase $\phi_{\mathrm{rec}} = x, -x, -x, x,$ +States–TPPI. The T_2 experiment (**b**) uses the same levels and durations of the gradient pulses as used in the T_1 experiment (**a**), and the phase cycle is the same as in (**a**). During CPMG pulse trains, the ^{15}N 180° pulses are applied every 0.9 ms and ^{1}H 180° pulses are applied every 4 ms. The ^{1}H 180° pulses are calibrated to ~40 μs corresponding to a field of 3.4 kHz to avoid sample heating problems. (**c**) The saturation in both NOE and NONOE experiments is achieved by applying ^{1}H 120° pulses every 5 ms for 3 s. The gradient pulses are used as $g_1 = 3$ ms, -20 G cm^{-1}, $g_2 = 1.25$ ms, 30 G cm^{-1}, $g_3 = g_4 = 0.5$ ms, 4 G cm^{-1}, $g_5 = 0.125$ ms, 27.8 G cm^{-1}. The phase cycle is $\phi_2 = y$ + States–TPPI, $\phi_3 = x, y, -x, -y$, $\phi_4 = x$, and receiver phase $\phi_{\mathrm{rec}} = x, -x,$ +States–TPPI. The saturation frequency is placed off-resonance for NONOE and switched back to on-resonance before the first ^{1}H 180° pulse. The phase of the last ^{1}H 90° pulse is used to ensure the water magnetization is along the z axis (not the $-z$ axis) immediately before acquisition (Farrow et al. 1994)

$$\xrightarrow{2\tau_1} -\xi 2\mathrm{H}_z\mathrm{N}_x \cos(\Omega_\mathrm{N} t_1) - \xi 2\mathrm{H}_z\mathrm{N}_y \sin(\Omega_\mathrm{N} t_1)$$

Both components are retained to generate two time domain data sets by the PEP sequence:

$$\begin{aligned}
&\xrightarrow{\left(\frac{\pi}{2}\right)(\mathrm{H}_x + \mathrm{N}_x)} \xi 2\mathrm{H}_y\mathrm{N}_x \cos(\Omega_\mathrm{N} t_1) + \xi 2\mathrm{H}_y\mathrm{N}_z \sin(\Omega_\mathrm{N} t_1)\\
&\xrightarrow{\tau\to\pi(\mathrm{H}_x + \mathrm{N}_x)\to\tau} \xi 2\mathrm{H}_y\mathrm{N}_x \cos(\Omega_\mathrm{N} t_1) - \xi \mathrm{H}_x \sin(\Omega_\mathrm{N} t_1)\\
&\xrightarrow{\left(\frac{\pi}{2}\right)(\mathrm{H}_y + \mathrm{N}_y)} -\xi 2\mathrm{H}_y\mathrm{N}_z \cos(\Omega_\mathrm{N} t_1) - \xi \mathrm{H}_z \sin(\Omega_\mathrm{N} t_1)\\
&\xrightarrow{\tau\to\pi(\mathrm{H}_x + \mathrm{N}_x)\to\tau\to\left(\frac{\pi}{2}\right)\mathrm{H}_x} \xi \mathrm{H}_x \cos(\Omega_\mathrm{N} t_1) + \xi \mathrm{H}_y \sin(\Omega_\mathrm{N} t_1)
\end{aligned} \tag{8.40}$$

The second FID is obtained by inverting both phase ϕ and the sign of gradient factor κ:

$$\xi \mathrm{H}_x \cos(\Omega_\mathrm{N} t_1) - \xi \mathrm{H}_y \sin(\Omega_\mathrm{N} t_1) \tag{8.41}$$

The two FIDs are recorded for a given t_1 value and stored in separate memory locations. The data are manipulated as described in Chap. 5 for the seHSQC to obtain pure phase data, which are processed using the States–TPPI method.

8.2.1.2 Experiment Setup and Data Processing

In addition to the setup procedure common to 2D heteronuclear experiments such as 90° pulse calibrations for transmitter and decoupler and spectral window selection, the typical setup for heteronuclear T_1 relaxation measurement includes a recycle delay set to 1.5–2.0 s; an array of 8–12 T delays ranging from 5 ms to 1.5 s; for ^{15}N, the delay τ for the INEPT sequence set to 2.25 ms [$<1/(4J_{\mathrm{XH}}) = 2.75$ ms], τ_1 set to 2.75 ms [$=1/(4J_{\mathrm{XH}})$], τ'_1 and τ''_1 are set according to the figure legend (Fig. 8.2) and the delay δ_2 is usually set to 0.5 ms. During period T, 180° shaped pulses selected for amide protons (or 120° hard ^{1}H pulses) are spaced at 5-ms intervals to eliminate the effects of dipole/CSA cross-correlation and cross-relaxation. The gradient pulses are set to 2 ms with ~10 G cm^{-1} for residual water suppression (g_3), 1 and 0.1 ms with ~30 G cm^{-1} for coherence dephase (g_6) and refocus (g_9), respectively, and 0.5 ms with 4–8 G cm^{-1} for all other gradients. The carrier frequency is set to the water resonance for ^{1}H and 118 ppm for the ^{15}N dimension. The data are acquired with 128 complex t_1 (^{15}N) increments and 1,024 complex t_2 (^{1}H) points, with the same spectral windows in ppm for ^{1}H (~15 ppm) and ^{15}N (~35 ppm) in all data sets.

Prior to Fourier transformation, it is necessary to rearrange the data according to the procedure described in Sect. 5.1.3 (PEP seHSQC). The arranged PEP data can be

processed separately as States–TPPI data and then the resulting in spectra combined together, or the data sets can be combined first and then processed in the conventional manner for States–TPPI. Prior to Fourier transformation, the FIDs are first multiplied by a 90°-shifted squared sine-bell or Gaussian window function and zero-filled twice to yield a digital resolution better than 2 Hz/point. A 90°-shifted squared sine-bell window function is applied to the indirect ^{15}N dimension. The data are zero-filled twice before the second Fourier transformation is applied. In general, linear prediction to improve digital resolution of the indirect dimension is not used since it may introduce a deviation from the real value of the T_1 relaxation rate. Each of the series of spectra is phase-corrected after being Fourier transformed: phase of ^{1}H dimension is adjusted according to the phase of the first FID of the shuffled data, whereas the phase of the ^{15}N dimension is corrected using two F_1 slices. The amplitudes of the cross-peaks are measured using either peak volume integrals or intensities if signal overlapping becomes severe. The intensity or volume integral $I_j(T)$ of the cross-peak for residue j is measured for all spectra with different values of T. The longitudinal relaxation time constant is calculated by fitting (1.83b) in Chap. 1 for all $I_j(T)$ values with the approximation that $I_{0j} = I_j(1.5\text{ s})$.

8.2.2 T_2 and $T_{1\rho}$ Measurements

8.2.2.1 Sensitivity-Enhanced HSQC for T_2 and $T_{1\rho}$ Measurements

The sequence for T_2 measurement (Fig. 8.2b, Farrow et al. 1994; Messerlie et al. 1989) is identical to the sequence used for T_1 measurement if the inversion scheme is replaced with a CPMG or spin lock sequence (Carr and Purcell 1954; Meiboom and Gill 1958). Rather than decaying along the longitudinal direction, the heteronuclear magnetization relaxes on the transverse plane during the T period of the T_2 pulse sequence. In addition to spin–spin interactions, the inhomogeneity of the magnetic field also contributes to the transverse relaxation. To remove the effect of field inhomogeneity, a CPMG spin echo sequence, which was developed by Carr and Purcell, and by Meiboom and Gill, is frequently applied in the measurement of transverse relaxation. In the CPMG scheme, the heteronuclear magnetization S_x evolves during a period ε under the interaction of the chemical shift and field inhomogeneity. After the 180° ^{15}N pulse reverses the direction of precession of the nuclear spins, the evolution due to the chemical shift and field inhomogeneity is refocused during the second ε period, provided that the spins being refocused remain in the identical magnetic field during both ε periods. The resulting transverse magnetization at the end of an even number of echoes in a CPMG pulse train has an amplitude decayed according to:

$$I = I_0 e^{-TR_2} \tag{8.42}$$

in which $T = 2n(2\varepsilon + \mathrm{pw}_{180^\circ})$, n is an integer and pw_{180° is the pulse length of a 180° ^{15}N pulse in the CPMG pulse train.

In the $R_{1\rho}$ experiment, the transverse magnetization is locked in the rotating frame by applying a spin lock train or continuous radio frequency field (Peng et al. 1991; Desvaux and Berthault 1999). The relaxation rate constant of the magnetization along the effective field direction in the rotating frame is called $R_{1\rho}$. The $R_{1\rho}$ measurement depends on such experimental parameters as the amplitudes of the applied B_1 field, ω_1, and the effective field in the rotating frame, ω_e, and the offset frequency Ω, $\omega_e^2 = \Omega^2 + \omega_1^2$. In the rotating frame, the tilt angle of the effective field from the RF field is given by:

$$\tan\theta = \frac{\omega_1}{\Omega} \tag{8.43}$$

The measured $R_{1\rho}$ is the combination of R_1 and R_2 via the dependence of the tilt angle:

$$R_{1\rho} = R_2 \sin^2\theta + R_1 \cos^2\theta \tag{8.44}$$

For an on-resonance spin lock field, θ is close to 90° for all resonances and the effective field is along the applied B_1 field (Meiboom 1961; Szyperski et al. 1993). The measured $R_{1\rho}$ represents the transverse relaxation rate constant R_2. For off-resonance $R_{1\rho}$ experiment (Akke and Palmer 1996; Zinn-Justin et al. 1997; Mulder et al. 1998), the RF transmitter frequency is placed far enough off-resonance so that θ in (8.43) is less than 70°. A pair of adiabatic ramp pulses is used to align the magnetization along the spin lock axis and rotate it back to the original direction. The magnetization at the beginning and the end of spin lock period is along the z axis. A continuous and small increase in the amplitude of the RF field causes the magnetization to follow the effective field in an adiabatic manner, resulting in a rotation, instead of projection, of the magnetization. At the end of the spin lock, the magnetization follows the effective field, by decreasing the amplitude of the B_1 field, back to the z axis.

In both the R_2 and $R_{1\rho}$ experiments, the two PEP FIDs obtained in the same manner to those obtained in the T_1 seHSQC sequence are given by:

$$\begin{aligned} &\xi \mathrm{H}_x \cos\left(\Omega_\mathrm{N} t_1\right) + \xi \mathrm{H}_y \sin(\Omega_\mathrm{N} t_1) \\ &\xi \mathrm{H}_x \cos\left(\Omega_\mathrm{N} t_1\right) - \xi \mathrm{H}_y \sin(\Omega_\mathrm{N} t_1) \end{aligned} \tag{8.45}$$

in which $\xi = \mathrm{e}^{-TR_2}$. The two FIDs are recorded for each given t_1 value and stored in separate memory locations. The data are treated as described in Sect. 5.1.3 for the PEP seHSQC to obtain pure phase data, which are processed using the States–TPPI method.

Analogous to the T_1 measurement, the contribution to the T_2 from cross-correlation of dipole/CSA is required to be minimized during the CPMG spin echo. The cross-correlation effect can be effectively removed by the combination of applying 180° ^{15}N pulses every 0.9 ms ($\varepsilon = 0.45$ ms) during the entire CPMG pulse train and applying 180° ^{1}H pulse centered in the CPMG pulse train. An alternative way is to apply 180° ^{15}N pulses every 0.9 ms and 180° ^{1}H pulses every 4 ms during the CPMG pulse train.

8.2.2.2 Experiment Setup and Data Processing

The setup procedure for the heteronuclear T_2 relaxation measurement is primarily identical to the procedure for T_1 relaxation measurement except for the setup of parameters for the relaxation period T. The number of echo cycles must be chosen as $2n$, in which n is an integer to ensure that the magnetization has same sign after the echo period. An array of 8–12 relaxation delays ranging from 5 to 150 ms is typically used. The time of the CPMG pulse train is set to be shorter than 150 ms to avoid sample heating problems caused by the pulse train. For the same reason, the ^{15}N RF field strength is set to less than 6 kHz, corresponding to a 90° ^{15}N pulse length of longer than 40 μs. As described previously, in order to remove the cross-correlation effect, a combination of 180° ^{15}N pulses every 0.9 ms during the entire CPMG pulse train and 180° ^{1}H pulses centered in the CPMG pulse train is applied. A different approach is also often used by applying 180° ^{15}N pulses every 0.9 ms and applying 180° (or 120°) ^{1}H pulses every 4–5 ms during the CPMG pulse train. The gradient pulse length and amplitude are the same as used in the T_1 experiment.

In the $R_{1\rho}$ experiment, the ^{15}N spin lock replaces the CPMG spin echo in the T_2 experiment, and is applied with a continuous RF ^{15}N pulse with a field strength less than 3.5 kHz to minimize sample heating problems. The sample heating during the spin lock can also be minimized by using a predelay time longer than 3 s. During the spin lock, 180° ^{1}H pulses spaced at 5-ms intervals are applied to eliminate the effects of dipole/CSA cross-correlation and cross-relaxation.

The data are processed in the same procedure as described for T_1 measurement after the rearrangement of the data according the procedure for PEP FIDs. Fitting for $T_{1\rho}$ values is required for the correction of the resonance offset effect (Peng and Wagner 1994).

8.2.3 Heteronuclear NOE Measurement

8.2.3.1 Heteronuclear NOE Experiment

The heteronuclear NOE is determined from the change in intensity of the NMR signal of heteronucleus X when the equilibrium magnetization of protons in the vicinity is perturbed by saturation in experiments such as the transient NOE or

steady-state NOE. The pulse sequence of a steady-state heteronuclear NOE experiment shown in Fig. 8.2c utilizes a pulse train to saturate proton equilibrium magnetization prior to the heteronuclear magnetization being excited. The first 90° ^{1}H pulse combined with the gradient is used to ensure that the ^{15}N magnetization is the only initial magnetization of the experiment. After the first 90° X pulse, the chemical shift of the heteronucleus X evolves during t_1 and the heteronuclear magnetization is transferred to proton with decoupling of the scalar coupling J_{XH}. In the final stage of the pulse sequence, the two orthogonal transverse magnetization components generated during t_1 are refocused by the PEP sequence for simultaneous detection by inverting the phase of ϕ_4 and sign of κ. The two FIDs are recorded and stored in separated memory locations. Quadrature detection in the F_1 dimension is obtained by shifting the phases of ϕ_2 and the receiver for each FID in a States–TPPI manner (see Sect. 4.10.2). To measure the NOE, a pair of experiments is recorded with the saturation (NOE) and without the saturation (NONOE) of the protons bound to the heteronuclei. The intensity of the heteronuclear NOE can be obtained from the longitudinal magnetization and relaxation rates of the heteronucleus X and proton H, which is the ratio of signal intensities between the NOE and NONOE (unsaturation) spectra (Goldman 1998: Farrow et al. 1994):

$$I_{\text{sat}} = \langle X_z \rangle_{\text{eq}} + \frac{\sigma_{XH}}{R_1} \langle H_z \rangle_{\text{eq}} = I_{\text{unsat}} \left(1 + \frac{\sigma_{XH}}{R_1} \frac{\gamma_H}{\gamma_X} \right) \tag{8.46}$$

in which I_{sat} and I_{unsat} represent the measured intensities of a resonance in the presence and absence of proton saturation, respectively; σ_{XH} is the rate constant of cross-relaxation; γ_X and γ_H are the gyromagnetic ratios. The values of NOE in (8.4) are obtained by the steady-state NOE values which are determined by the ratios of the peak intensities in the NOE and NONOE spectra:

$$\text{NOE} = \frac{I_{\text{sat}}}{I_{\text{unsat}}} = 1 + \frac{\sigma_{XH}}{R_1} \frac{\gamma_H}{\gamma_X} \tag{8.47}$$

The standard deviation of NOE value, $\overline{\delta}_{\text{NOE}}$ can be determined using the measured background noise levels:

$$\frac{\overline{\delta}_{\text{NOE}}}{\text{NOE}} = \sqrt{\frac{\overline{\delta}^2_{\text{sat}}}{I^2_{\text{sat}}} + \frac{\overline{\delta}^2_{\text{unsat}}}{I^2_{\text{unsat}}}} \tag{8.48}$$

in which $\overline{\delta}_{\text{sat}}$ and $\overline{\delta}^2_{\text{unsat}}$ represent the standard deviations of I_{sat} and I_{unsat}, respectively, calculated from the root-mean-squared noise of background regions (Nicholson et al. 1992). In the condition of the extreme narrowing limit ($\omega\tau_m \ll 1$) in which τ_m is short, $\sigma_{XH} = \frac{1}{2}R_1$ which yields a maximum magnitude of NOE. Therefore, ^{15}N spins have NOE values between 1 and −4 because of its negative gyromagnetic ratio, whereas ^{13}C NOE values are in the range of 1–5.

The magnetization transfer in the experiment can be described by product operators. The transverse ^{15}N magnetization is frequency-labeled and transferred to ^{1}H spins during the first period:

$$\begin{aligned} \mathrm{N}_z &\xrightarrow{\left(\frac{\pi}{2}\right)\mathrm{N}_x} \mathrm{N}_y \xrightarrow{t_1} \mathrm{N}_y \cos\left(\Omega_\mathrm{N} t_1\right) - \mathrm{N}_x \sin\left(\Omega_\mathrm{N} t_1\right) \\ &\xrightarrow{2\tau_1} -2\mathrm{H}_z\mathrm{N}_x \cos\left(\Omega_\mathrm{N} t_1\right) - 2\mathrm{H}_z\mathrm{N}_y \sin\left(\Omega_\mathrm{N} t_1\right) \end{aligned} \tag{8.49}$$

The scalar coupling J_{XH} is refocused during the t_1 evolution time if τ_1 is set to $1/(4J_{\mathrm{XH}})$. Both orthogonal components of the ^{1}H magnetization are refocused and observed by the PEP sequence (8.40), resulting in the two FIDs:

$$\begin{aligned} &\mathrm{H}_x \cos\left(\Omega_\mathrm{N} t_1\right) + \mathrm{H}_y \sin\left(\Omega_\mathrm{N} t_1\right) \\ &\mathrm{H}_x \cos\left(\Omega_\mathrm{N} t_1\right) - \mathrm{H}_y \sin(\Omega_\mathrm{N} t_1) \end{aligned} \tag{8.50}$$

8.2.3.2 Experiment Setup and Data Processing

The saturation of the ^{1}H magnetization is obtained by applying either 120° ^{1}H pulses every 5 ms for 3 s or a WALTZ16 pulse train for 3 s. The 90° ^{1}H pulse length for the WALTZ16 is calibrated to about 30 μs. A total recycle time of at least 5 s is used for ^{15}N measurement to allow the longitudinal magnetization to relax back to equilibrium. Usually, the NOE and NONOE spectra are recorded in an interleaved manner to reduce artifacts. The gradient amplitude and durations are selected as $g_1 = 3$ ms, -20 G cm^{-1}; $g_2 = 1.25$ ms, 30 G cm^{-1}; $g_3 = g_4 = 0.5$ ms, 4 G cm^{-1}; $g_5 = 0.125$, 27.8 G cm^{-1}. The delays are set to $\tau = 2.25$ ms, $\tau_1 = 2.75$ ms, and $\delta_2 = 0.5$ ms. A total of 128 complex t_1 points is usually recorded.

After rearrangement of the PEP data, the FIDs are processed into a 512 × 1,024 matrix with 90°-shifted squared sine-bell window functions in both dimensions. The ^{15}N NOE values are calculated from the ratio $I_{\mathrm{sat}}/I_{\mathrm{unsat}}$ of the cross-peak intensities (8.47) in the NOE and NONOE spectra.

8.3 Relaxation Data Analysis

The R_1 and R_2 values are obtained by fitting the intensities of individual cross-peaks with a series of values of relaxation times T using (1.83b) and (8.42), respectively. The NOE values are extracted from the intensity ratios of individual cross-peaks in the NOE and NONOE experiments using (8.47) for the data recorded at different static magnetic field strengths. Once the values of the relaxation rates and NOE are

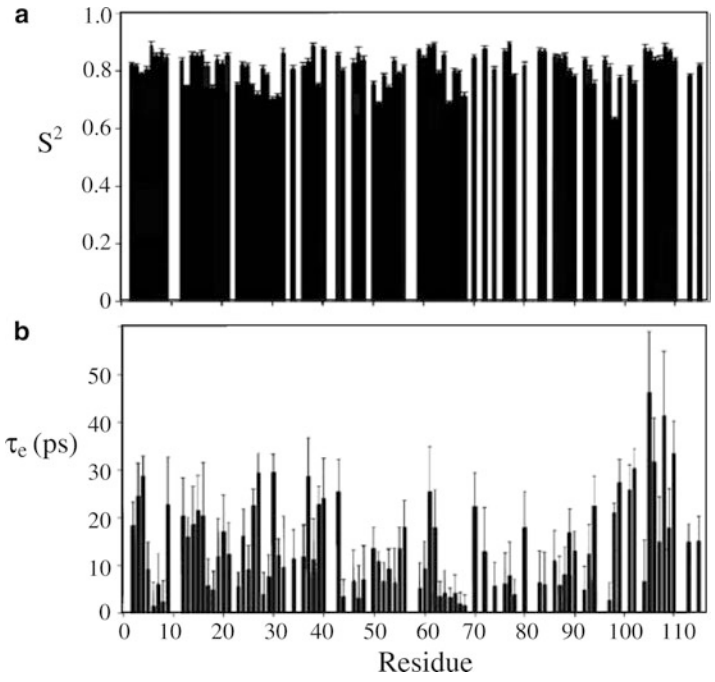

Fig. 8.3 Simple model-free parameters for local motion of the backbone amide N–H of ferrocytochrome *c*2 derived from ^{15}N relaxation data recorded at 30 °C and analyzed using an axially symmetric diffusion tensor. (**a**) Squared generalized order parameters (S^2). (**b**) Effective correlation time constants (reproduced with permission from Flynn et al. (2001), Copyright © 2001American Chemical Society)

calculated, the overall correlation time τ_m is usually determined from the 10 % trimmed mean of the R_2/R_1 ratio (Mandel et al. 1995). In the next step, dynamic parameters (squared generalized order parameter S^2, and τ_c) are obtained via such methods described in the theory section as a grid search by minimizing the global error function or local error functions using the estimated τ_m value (Mandel et al. 1995; Dellow and Wand 1989). The program CurveFit is available for determining R_1 and R_2 from experimental data, and the program "Modelfree" can be used to fit the R_1 and R_2 and NOE data to heteronuclear relaxation data to obtain model-free parameters according to the extended model-free formalism using minimization of the error function (http://cpmcnet.columbia.edu/dept/gsas/biochem/labs/palmer/).

Once S^2 and τ_e are obtained, interpretation of the results is straightforward. The dynamic parameters can be plotted for each residue as shown in Fig. 8.3. Backbone and side-chain dynamics information can be obtained based on the distribution of S^2 and τ_e over the residues. As mentioned earlier, S^2 with higher amplitude indicates that the motion of the bond vector is restricted to the rigid orientations. As S^2 decreases, the motion of the bond vector becomes less restricted. The motion becomes completely isotropic as S^2 approaches zero. In addition to S^2, the internal

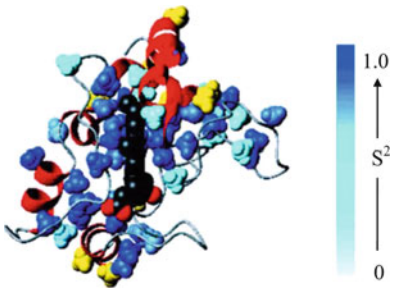

Fig. 8.4 S^2 axis parameters colored-coded on the structure of ferrocytochrome $c2$ (reproduced with permission from Flynn et al. (2001), Copyright © 2001 American Chemical Society)

correlation time τ_e characterizes how fast the internal motion is. As the example in Fig. 8.3 indicates, the majority of the amide NH S^2 are distributed near 0.8 with the corresponding effective correlation times in the range of 1–50 ps. The obtained model-free parameters of the protein are basically consistent with a well-ordered polypeptide backbone. The values of S^2 can be color-coded on the structure (Fig. 8.4), which provides visualization of the backbone or side-chain dynamics. Several backbone regions between regular secondary structure elements have slightly lower order parameters (0.7 ± 0.05). Overall, the backbone dynamics of ferrocytochrome $c2$ reveals that the interior of the protein is unusually rigid.

Questions

1. What are the experimental parameters measured for the study of protein dynamics?
2. What are the two methods for calculating the spectral density functions from experimental data using model-free analysis?
3. What is the assumption of model-free analysis?
4. What is the physical meaning of the squared generalized order parameters S^2? What is the range of S^2 value? What kind of motion does an S^2 with a value near 0.8 describe?
5. What is the relationship of R_1, R_2, and $R_{1\rho}$?
6. Derive (8.22) and (8.23) from (8.14) and (8.15) using (8.20) and (8.21), and $\beta_1 = 0.921$ and $\beta_2 = 0.955$ for ^{15}N. Hint: derive (8.23) first. $J(\omega_X)$ in (8.14) and (8.15) equals $J(\omega_N)$. To derive (8.22) for ^{15}N, substitute $J(\omega_N)$ with (8.23).

References

Abragam A (1961) Principles of nuclear magnetism. Clarendon Press, Oxford

Akke M, Palmer G (1996) Monitoring macromolecular motions on microsecond to millisecond time scales by R1ρ−R1 constant relaxation time NMR spectroscopy. J Am Chem Soc 118:911–912

Brüschweiler R, Liao X, Wright PE (1995) Long-range motional restrictions in a multidomain zinc-finger protein from anisotropic tumbling. Science 268:886–889

Bull TE (1992) Relaxation in the rotating frame in liquids. Prog Nucl Magn Reson Spectrosc 24:377–410

Carr HY, Purcell EM (1954) Effects of diffusion on free precession in nuclear magnetic resonance experiments. Phys Rev 94:630–638

Clore GM, Szabo A, Bax A, Kay LE, Driscoll PC, Gronenborn AM (1990a) Deviations from the simple two-parameter model-free approach to the interpretation of nitrogen-15 nuclear magnetic relaxation of proteins. J Am Chem Soc 112:4989–4991

Clore GM, Driscoll PC, Wingfield PT, Gronenborn AM (1990b) Analysis of the backbone dynamics of interleukin-1.beta. using two-dimensional inverse detected heteronuclear nitrogen-15-proton NMR spectroscopy. Biochemistry 29:7387–7401

Dayie KT, Wagner G, Lefevre JF (1996) Theory and practice of nuclear spin relaxation in proteins. Annu Rev Phys Chem 47:243–282

Dellwo MJ, Wand AJ (1989) Model-independent and model-dependent analysis of the global and internal dynamics of cyclosporin A. J Am Chem Soc 111:4571–4578

Desvaux H, Berthault P (1999) Study of dynamic processes in liquids using off-resonance rf irradiation. Prog Nucl Magn Reson Spectrosc 35:295–340

Farrow NA, Zhang O, Szabo A, Torchoia DA, Kay LE (1995) Spectral density function mapping using 15N relaxation data exclusively. J Biomol NMR 6:153–162

Farrow NA, Muhandiram R, Singer AU, Pascal SM, Kay CM, Gish G, Shoelson SE, Pawson T, Forman-Kay JD, Kay LE (1994) Backbone dynamics of a free and a phosphopeptide-complexed Src homology 2 domain studied by 15N NMR relaxation. Biochemistry 33:5984–6003

Flynn PF, Bieber Urbauer RJ, Zhang H, Lee AL, Wand AJ (2001) Main chain and side chain dynamics of a heme protein: 15N and 2H NMR relaxation studies of R. capsulatus ferrocytochrome c2. Biochemistry 40:6559–6569

Goldman M (1984) Interference effects in the relaxation of a pair of unlike spin-1/2 nuclei. J Magn Reson 60:437–452

Hiyama Y, Niu C, Silverton JV, Bavoso A, Torchia DA (1988) Determination of 15N chemical shift tensor via 15N-2H dipolar coupling in Boc-glycylglycyl[15N glycine]benzyl ester. J Am Chem Soc 110:2378–2383

Ishima R, Torchia DA (2000) Protein dynamics from NMR. Nat Struct Biol 7:740–743

Ishima R, Nagayama K (1995a) Protein backbone dynamics revealed by quasi spectral density function analysis of amide N-15 nuclei. Biochemistry 34:3162–3171

Ishima R, Nagayama K (1995b) Quasi-spectral-density function analysis for nitrogen-15 nuclei in proteins. J Magn Reson B108:73–76

Kay LE, Torchia DA, Bax A (1989) Backbone dynamics of proteins as studied by 15N inverse detected heteronuclear NMR spectroscopy: application to staphylococcal nuclease. Biochemistry 28:8972–8979

Kay LE, Keifer P, Saarinen T (1992) Pure absorption gradient enhanced heteronuclear single quantum correlation spectroscopy with improved sensitivity. J Am Chem Soc 114:10663–10665

Kroenke CD, Rance M, Palmer AG III (1999) Variability of the 15N chemical shift anisotropy in Escherichia coli Ribonuclease H in solution. J Am Chem Soc 121:10119–10125

Lipari G, Szabo A (1982a) Model-free approach to the interpretation of nuclear magnetic resonance relaxation in macromolecules. 1. Theory and range of validity. J Am Chem Soc 104:4546–4559

Lipari G, Szabo A (1982b) Model-free approach to the interpretation of nuclear magnetic resonance relaxation in macromolecules. 2. Analysis of experimental results. J Am Chem Soc 104:4559–4570

London RE (1980) Intramolecular dynamics of proteins and peptides as monitored by nuclear magnetic relaxation experiments. in Magnetic Resonance in Biology, J.S. Cohen (ed.), Wiley, New York, pp. 1–69

Mandel AM, Akke M, Palmer AG III (1995) Backbone dynamics of Escherichia coli ribonuclease HI: correlations with structure and function in an active enzyme. J Mol Biol 246:144–163

Mayo KH, Daragan VA, Idiyatullin D, Nesmelova I (2000) Peptide internal motions on nanosecond time scale derived from direct fitting of 13C and 15N NMR spectral density functions. J Magn Reson 146:188–195

Meiboom S, Gill D (1958) Modified spin-echo method for measuring nuclear relaxation times. Rev Sci Instrum 29:688–691

Meiboom S (1961) Nuclear magnetic resonance study of the proton transfer in water. J Chem Phys 34:375–388

Messerlie BA, Wider G, Otting G, Weber C, Wuthrich K (1989) Solvent suppression using a spin lock in 2D and 3D NMR spectroscopy with H2O solutions. J Magn Reson 85:608–613

Mulder FAA, de Graaf RA, Kaptein R, Boelens R (1998) An off-resonance rotating frame relaxation experiment for the investigation of macromolecular dynamics using adiabatic rotations. J Magn Reson 131:351–357

Nicholson LK, Kay LE, Baldisseri DM, Arango J, Young PE, Torchia DA (1992) Dynamics of methyl groups in proteins as studied by proton-detected carbon-13 NMR spectroscopy. Application to the leucine residues of staphylococcal nuclease. Biochemistry 31:5253–5263

Palmer AG III (2001) NMR probes of molecular dynamics: overview and comparison with other techniques. Annu Rev Biophys Biomol Struct 30:129–155

Palmer AG III, Rance M, Wright PE (1991) Intramolecular motions of a zinc finger DNA-binding domain from Xfin characterized by proton-detected natural abundance carbon-13 heteronuclear NMR spectroscopy. J Am Chem Soc 113:4371–4380

Peng JW, Wagner G (1994) Protein Mobility from Multiple ^{15}N relaxation Parameters in Tycko R (ed.) Nuclear Magnetic Resonance Probes of Molecular Dynamics. Kluwer, Dordrecht, pp. 373–454

Peng JW, Wagner G (1995) Frequency spectrum of NH bonds in eglin c from spectral density mapping at multiple fields. Biochemistry 34:16733–16752

Peng JW, Thanabal V, Wagner G (1991) 2D heteronuclear NMR measurements of spin–lattice relaxation times in the rotating frame of X nuclei in heteronuclear HX spin systems. J Magn Reson 94:82–100

Phan IQ, Boyd J, Campbell ID (1996) Dynamic studies of a fibronectin type I module pair at three frequencies: anisotropic modelling and direct determination of conformational exchange. J Biomol NMR 8:369–378

Szyperski T, Luginbul P, Otting G, Guntert P, Wuthrich K (1993) Protein dynamics studied by rotating frame 15N spin relaxation times. J Biomol NMR 3:151–164

Wittebort R, Szabo A (1978) Theory of NMR relaxation in macromolecules: restricted diffusion and jump models for multiple internal rotations in amino acid side chains. J Chem Phys 69:1722–1736

Yamazaki T, Muhandiram R, Kay LE (1994) NMR experiments for the measurement of carbon relaxation properties in highly enriched, uniformly 13C, 15N-labeled proteins: application to 13Cα carbons. J Am Chem Soc 116:8266–8278

Ye C, Fu R, Hu J, Hou L, Ding S (1993) Carbon-13 chemical shift anisotropies of solid amino acids. Magn Reson Chem 31:699–704

Zinn-Justin S, Berthault P, Guenneuges M, Desvaux H (1997) Off-resonance rf fields in heteronuclear NMR: application to the study of slow motions. J Biomol NMR 10:363–372